

Diffusion Kinetics of Samarium and Neodymium in Garnet, and a Method for Determining Cooling Rates of Rocks

J. Ganguly, M. Tirone, R. L. Hervig

Experimental determinations of the diffusion coefficients of samarium and neodymium in almandine garnet and theoretical considerations show that one cannot assign a sufficiently restricted range of closure temperature, T_C , to the samarium-neodymium decay system in garnet for the purpose of constraining the cooling rate. However, it is shown that the samarium-neodymium cooling age of garnet can be used to calculate both cooling rate and T_C if the temperature and age at the peak metamorphic conditions are known.

Garnets in metamorphic rocks are important candidates for radiometric age determinations through use of U-Pb, Rb-Sr, and Sm-Nd decay systems. Knowledge of the temperatures at which these systems closed in a garnet crystal with respect to element diffusion would provide important constraints on the cooling and exhumation history of the host rock. The T_C of the Sm-Nd system in metamorphic garnet has been a subject of continued debate, with the estimates varying from $\sim 400^\circ$ to 800°C (1-6). We present experimental data on values of the tracer diffusion coefficient (D) of Sm and Nd in garnet and apply them to address the problems of closure temperature and cooling rates.

The diffusion experiments were carried out at a pressure of 1 bar and temperature of 777° to 827°C for ~ 146 to 48 hours. Natural almandine crystals ($\text{Alm}_{75}\text{Py}_{25}$) were polished on one side to a mirror finish by a combination of mechanical and chemical polishing (7) and then thermally annealed for at least 8 hours at or close to the T - $f\text{O}_2$ (oxygen fugacity) condition of the experiment so that it had an equilibrium or nearly equilibrium defect concentration for the experimental condition. A drop of a solution (8) consisting of both ^{149}Sm and ^{145}Nd (~ 100 to 200 parts per million of each) was added to the polished surface of a crystal. After drying, the crystal was suspended inside a vertical gas-mixing furnace, which was preheated to a desired temperature. The $f\text{O}_2$ was controlled by a computer-regulated CO-CO₂ mixture and was maintained at the wüstite-iron (WI) buffer (9), with the exception of one experiment at 800°C , which was conducted at 2.1 logarithmic units above this buffer (the approximate limit of almandine stability) to test

the effect of $f\text{O}_2$ on the diffusion. On completion of an annealing experiment, the sample was cleaned by sonication in 2 to 4 N HCl solution and rubbing on a soft polishing cloth with ethanol to remove as much of the residual solution from the sample surface as possible, and analyzed by depth profiling with an ion probe (10). The polished surface of an annealed crystal appeared very shiny in reflected light under an optical microscope, suggesting that there was no chemical reaction between the crystal and the diffusant layer.

The samples were also analyzed simultaneously for ^{145}Nd , ^{149}Sm , ^{30}Si , ^{89}Y , and ^{35}Cl (Fig. 1). The depth profiles for the nondiffusing species ^{30}Si and ^{89}Y allowed monitoring of the stability of analyses, whereas that of ^{35}Cl (absent in garnet) allowed location of the crystal surface. Plateau intensities for ^{89}Y and ^{30}Si were not achieved for several measurement cycles, and the count rates for the diffusants were ignored for these cycles. A control garnet sample, which was not subjected to diffusion anneal, showed the same stabilization behavior of ^{89}Y and ^{30}Si . The diffusion depths of ^{149}Sm and ^{145}Nd varied between ~ 1100 and 3000 \AA . The energetically most favorable diffusion mechanism of a tracer isotope is by replacement of the isotopes of the same element that are already present in the crystal.

Modeling was carried out in two ways. In the first, the crystal surface was assumed to have a fixed concentration of each diffusing species (semi-infinite reservoir model). In the second, the surface concentration of a diffusing species was allowed to deplete with time, t . Assuming constant D , solutions of the diffusion equation (11) for the two cases yield expressions of the concentration as a function of distance, $C(x)$, in terms of Dt and a constant term, A . We solved for both D and A simultaneously by incorporating the solutions into an optimization program (12). In all cas-

es, the semi-infinite source model yielded a better fit to the experimental data than the depleting source model. Modeling of the data from different depth profiles in the same sample or in different samples annealed at the same condition yielded D values that differed by a factor ≤ 1.6 . For constant D and diffusion in an isotropic medium, the unevenness of a diffusant layer deposited on a crystal surface does not affect the retrieved D value (13). Three time series experiments (18.4, 41.8, and 76 hours) at 877°C did not show any systematic dependence of $D(\text{Nd})$ and $D(\text{Sm})$ on time, thus satisfying an important condition for the validity of the diffusion data. The results of modeling the diffusion profiles show that the D for the slightly smaller cation (14) Sm (1.09 \AA) is 5 to 10% larger than that of Nd (1.12 \AA). These diffusion coefficients are similar to that of Mg, but about a factor of 10 larger than that of Fe at $f\text{O}_2$ of graphite-oxygen equilibrium (Fig. 2). The effect of $f\text{O}_2$ on D determined in this work is compatible with the predicted 1/6 power dependence of D on $f\text{O}_2$ (15, 16).

The T_C of the Sm-Nd decay system in garnet has previously been estimated empirically (2-5) or calculated (1, 6, 17) from the available diffusion data of Sm and Nd (18, 19). At 1 bar and $\sim 700^\circ\text{C}$, our $D(\text{Sm})$ is at least three orders of magnitude lower (Fig. 2) than that obtained by the extrapolation of the high P - T data of Harrison and Wood (18), which were derived as a by-product of the experimental results on Sm partitioning between garnet and melt. For comparison with our results, we adjusted Coghlan's data for

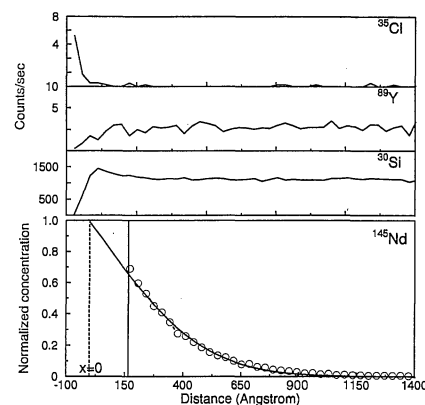


Fig. 1. Illustration of the depth profiles of the diffusing and nondiffusing isotopes. The crystal surface ($X = 0$) was located by monitoring ^{35}Cl , whereas simultaneous stabilization of ^{30}Si and ^{89}Y were used to select data for the diffusant (^{145}Nd) for use in the determination of the diffusion coefficient. All ^{145}Nd data have been normalized according to $[\text{Nd}(X) - \text{Nd}(\infty)] / [\text{Nd}(0) - \text{Nd}(\infty)]$, where X is the distance. The solid line through the data points is the calculated diffusion profile with $D = 1.3 \times 10^{-17} \text{ cm}^2/\text{s}$ at the experimental condition of 1 bar, 877°C , $f\text{O}_2 \equiv \text{WI}$ buffer. Data for ^{149}Sm data are indistinguishable from those of ^{145}Nd in the plot.

J. Ganguly and M. Tirone, Department of Geosciences, University of Arizona, Tucson, AZ 85721, USA. R. L. Hervig, Center for Solid State Science, Arizona State University, Tempe, AZ 85287, USA.

Nd diffusion (19) to the fO_2 condition of WI buffer, assuming that $D \propto (fO_2)^{1/6}$. These data, which are much lower than ours, are problematic for two reasons: the activation energy for $D(Nd)$ is 44 ± 7 kcal/mol, which is much lower than that (~ 60 to 70 kcal/mol) of the smaller divalent cations Mg, Fe, and Mn (7, 20); and the experiments were performed under hydrothermal condition (2 kb, Ni-NiO buffer), resulting in extensive surface dissolution of most garnets. It is possible that the apparently clean analyzed areas also suffered from dissolution or hydration reaction, but at a scale at which they could not be detected optically. In a reaction-diffusion process, one would determine an apparent diffusion coefficient that is smaller than the true one (11, eqn. 14.3). Observational data also suggest that $D(Nd)$ data of Coghlan are too low (4).

Dodson (21) derived an expression of T_C of a diffusing species in a mineral, assuming that it is surrounded by a semi-infinite homogeneous reservoir of that species. In a mineral with retrograde zoning, the species concentration "freezes" at progressively lower temperatures from the core to rim, so that this T_C is a weighted average of the values for T_C in

the different parts. Dodson (21, 22) also assumed that the composition of the mineral is sufficiently removed at all points from its initial homogeneous composition attained at the peak temperature, T_o . However, this assumption, which makes T_C independent of T_o , is not usually satisfied by slowly diffusing species, such as Sm and Nd in garnet. Using an extension (23) of Dodson's formulation that excludes this restriction and the diffusion data from this study, we calculated (Fig. 3) the mean T_C of Sm-Nd decay system in garnet as a function of grain size, cooling rate, and T_o at 7 kb and fO_2 of graphite-oxygen buffer. These conditions approximate the average conditions of metamorphic rocks in which garnet ages are often determined through use of the Sm-Nd decay system. Due to the lack of any data on the pressure dependence of their diffusion coefficients, we assumed that the rare-earth elements have the same activation volume, ΔV^+ , as Mn^{2+} (largest cation for which data are available in garnet), which is $6 \text{ cm}^3/\text{mol}$ (20), and that $D \propto (fO_2)^{1/6}$. We thus obtained an Arrhenian expression of D (7 kb, $fO_2 \equiv$ graphite buffer) = $D_o \exp[-Q(P)]/RT$ with $D_o = 4.7 \times 10^{-5} \text{ cm}^2/\text{s}$ and $Q(P) = Q(1\text{bar}) + P\Delta V^+ =$

61,674 cal/mol. It is evident from Fig. 3 that one cannot define a unique or even a restricted range of T_C of the Sm-Nd decay system in garnet, and that Dodson's formulation (21) progressively overestimates T_C with increasing cooling rate and grain size and decreasing T_o .

In addition to grain size, T_C is also sensitive to T_o , except at very slow cooling rate, but at this condition T_C is itself too sensitive to cooling rate to be useful in the reconstruction of the temperature-time path of a rock during cooling. However, the cooling rate of a rock can be retrieved by noting that any point on a curve in Fig. 3 defines T_o , T_C , and an average cooling rate within this temperature range, which is given by $(T_o - T_C)/\Delta t$, where Δt represents the difference between the peak metamorphic age and Sm-Nd cooling age of garnet (that is, the elapsed time until the Sm-Nd decay system closed within garnet crystals during cooling). Thus, if T_o , a , and Δt are known, one can find the point on the appropriate curve that satisfies the known value of Δt [given by the ratio of $(T_o - T_C)$ to the cooling rate defined by the point]. The coordinates of this point specify both T_C and the average cooling rate between T_o and T_C of the garnet.

As an example of application of the relation of the average cooling rate between T_o and T_C versus Δt , as derived according to the above analysis for different combinations of T_o and grain size (Fig. 4), we consider the data of Mezger *et al.* (3) for the Archean Pikwitonei Granulite Domain of the Superior Province, Canada. Using two-feldspar thermometry, they estimated $T_o \sim 750^\circ\text{C}$ for the peak metamorphism at ~ 2640 million years ago (Ma), as determined by U-Pb ages of zircon and garnet, which is ~ 30 Ma older than the Sm-Nd cooling age of garnet. In thin sections, the size (or apparent diameter) of the garnet crystals varied between ~ 1 and 5

Fig. 2. Comparison of the tracer diffusion coefficients of ^{149}Sm and ^{143}Nd (squares and triangles, respectively) in almandine garnet determined in this work at 1 bar (open symbols: $fO_2 \equiv$ WI buffer; symbol with cross above the Arrhenian fit: 2.1 log units above WI buffer) with other diffusion data in garnet. $D(\text{Mg})$ and $D(\text{Fe})$ are the self (\sim tracer) diffusion of Mg and Fe (7) at fO_2 of graphite- O_2 buffer (normalized to 1 bar). (Inset) Results of a time series study at 877°C ; the datum for the longest run is plotted in the main figure.

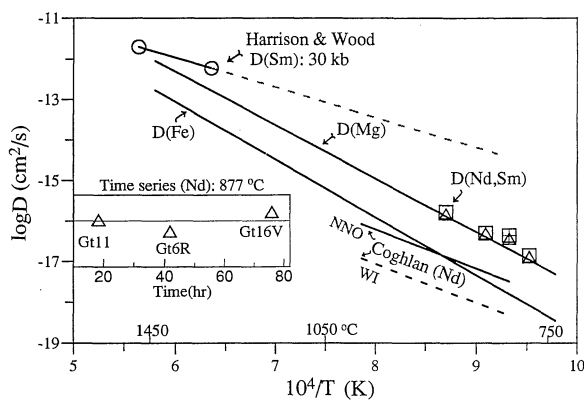
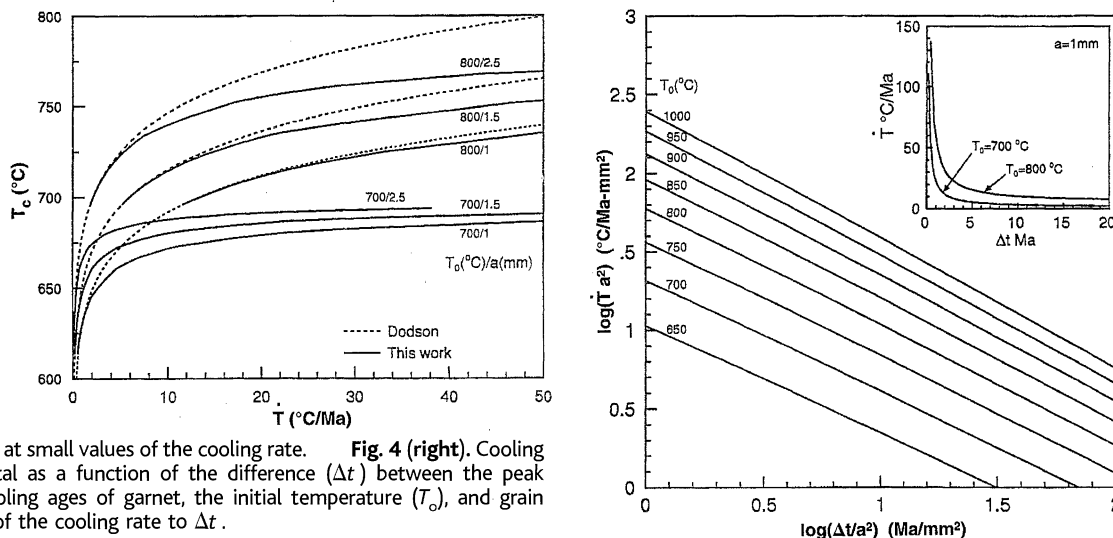


Fig. 3 (left). Closure temperature (T_C) of Sm-Nd decay system in spherical garnet (almandine) crystal as a function of cooling rate, initial temperature (T_o), and grain radius (a). Also shown (dashed lines) are the values of T_C calculated from Dodson (21), which are independent of T_o . Note the coincidence of the family of T_C versus cooling rate curves for a given grain size, as calculated here for different values of T_o , with the single curve for the same grain size calculated from (21) at small values of the cooling rate. **Fig. 4 (right).** Cooling rate of spherical garnet crystal as a function of the difference (Δt) between the peak metamorphic and Sm-Nd cooling ages of garnet, the initial temperature (T_o), and grain radius (a). (Inset) Sensitivity of the cooling rate to Δt .



mm. Using these data, we obtain from Fig. 4 cooling rate ~ 2 to 4 K/Ma, which is in excellent agreement with that of ~ 2 K/Ma deduced independently (3). For very slowly cooled rocks, the retrieved cooling rate is quite insensitive to errors in Δt . However, for relatively rapidly cooled rocks (for example, $dT/dt > 50$ K/Ma for $T_0 = 800^\circ\text{C}$), small error in Δt leads to very large error in dT/dt . Thus, for these rocks, it would be more appropriate to define a minimum cooling rate, taking into account the error in Δt .

References and Notes

1. F. J. Humphries and R. A. Cliff, *Nature* **295**, 515 (1982).
2. A. S. Cohen, R. K. O'Nions, R. Siegenthaler, W. I. Griffin, *Contrib. Mineral. Petrol.* **98**, 303 (1988).
3. K. Mezger, E. J. Essene, A. N. Halliday, *Earth Planet. Sci. Lett.* **113**, 387 (1992).
4. K. Burton, M. J. Kohn, A. S. Cohen, R. K. O'Nions, *ibid.* **133**, 199 (1992).
5. B. J. Hensen and B. Zhou, *Geology* **23**, 225 (1995).
6. H. Becker, *Contrib. Mineral. Petrol.* **127**, 224 (1997).
7. J. Ganguly, W. Cheng, S. Chakraborty, *ibid.* **131**, 171 (1998).
8. The isotope-enriched solution was prepared by first dissolving metals of Sm and Nd, enriched in the isotopes ^{149}Sm and ^{145}Nd , respectively, in 2 N HCl, evaporating it to almost dryness, and then adding triply distilled water. The nearly aqueous solutions were analyzed by inductively coupled plasma-mass spectrometry (ICP-MS) and found to have ^{145}Nd and ^{149}Sm concentrations varying between ~ 100 and 200 ppm in two different stock solutions used in this work.
9. H. St. C. O'Neill, *Am. Mineral.* **73**, 470 (1988).
10. The analyses were obtained in a Cameca ims 3f SIMS using a primary beam of mass-filtered $^{16}\text{O}^-$ accelerated to 10 keV. The samples were held at $\sim +4.5$ kV, resulting in an impact energy of ~ 14.5 keV. Two approaches were used to avoid contribution of secondary ions from the crater walls. For some of the samples, a 50-nA primary beam was focused onto a spot and rastered over a $200\ \mu\text{m}$ by $200\ \mu\text{m}$ area. An aperture inserted into the path of the ions allowed only those originating from a $60\text{-}\mu\text{m}$ -diameter circular area in the center of the crater into the mass spectrometer. For other samples, a 15- to 20-nA primary beam was focused by Kohler illumination to generate a circular, flat-bottomed crater $\sim 120\ \mu\text{m}$ in diameter (24). Secondary ions from the central 10 or $20\ \mu\text{m}$ of the crater were allowed into the mass spectrometer by selecting either a 100- or $200\text{-}\mu\text{m}$ field aperture. In both cases a 75-V offset was applied to the sample voltage to minimize the contribution of molecular ions to the mass spectrum (25). Crater depths were determined with a Dektak surface profilometer and varied as a function of primary beam current and analysis time (1 to 2 hours) between ~ 3000 and $7000\ \text{\AA}$.
11. J. Crank, *The Mathematics of Diffusion* (Clarendon, Oxford, 1975).
12. F. James and M. Ross, *Comput. Phys.* **10**, 343 (1975).
13. D. S. Tannhauser, *Appl. Phys.* **27**, 662 (1956).
14. R. D. Shannon and C. T. Prewitt, *Acta Crystallogr.* **B25**, 925 (1969).
15. S. Chakraborty and J. Ganguly, in *Diffusion, Atomic Ordering and Mass Transport*, J. Ganguly, Ed. (Advances in Physical Geochemistry 8, Springer-Verlag, New York, 1991), pp. 120–175.
16. M. Morioka and H. Nagasawa, in (15), pp. 176–197.
17. D. J. Cherniak, J. M. Manchar, E. B. Watson, *Chem. Geol.* **134**, 289 (1997).
18. W. J. Harrison and B. J. Wood, *Contrib. Mineral. Petrol.* **72**, 145 (1980).
19. R. A. N. Coghlan, thesis, Brown University, Providence, RI (1990).
20. S. Chakraborty and J. Ganguly, *Contrib. Mineral. Petrol.* **111**, 74 (1992).
21. M. H. Dodson, *ibid.* **40**, 259 (1973).
22. ———, *Mat. Sci. Forum* **7**, 145 (1986).
23. J. Ganguly, in preparation. The geometric parameter A in the expression of mean T_C in Dodson's (21) eqn. 23 equals $\exp(G)$, where G is the spatially averaged value of the closure function $G(x)$ of his (22) eqn. 20. In deriving the expression for $G(x)$, Dodson (22) assumed that the dimensionless quantity $M \gg 1$, which implies removal of the composition of the crystal from its initial composition in all parts. The closure function has been modified so that it is valid for any arbitrary value of M , numerically evaluated as a function of the normalized radial distance from the center of a grain, and then spatially averaged to yield average closure function versus M ; for example, $G(M = 0.001) = 0.9018$, $G(0.01) = 2.7603$, $G(0.10) = 3.8693$, $G(0.4) = 4.0041$, as compared to Dodson's (22) $G = 4.0066$.
24. S. W. J. Clement, W. Compston, G. Newstead, in *Proceedings International Secondary Ion Mass Spectrometry Conference*, A. Bennighoven, Ed. (Wiley, Münster, Germany, 1991), pp. 289–293.
25. E. K. Zinner and G. Crozaz, *Int. J. Mass Spectrom Ion* **69**, 17 (1986).
26. We thank M. H. Dodson and J. Ruiz for helpful discussions and for providing some of the isotope-enriched solutions, respectively. This research was supported by U.S. National Science Foundation grant EAR 9418941 and EAR 9805232.

30 April 1998; accepted 30 June 1998

Decoupled Temporal Patterns of Evolution and Ecology in Two Post-Paleozoic Clades

Frank K. McKinney,* Scott Lidgard, J. John Sepkoski Jr., Paul D. Taylor

Counts of taxonomic diversity are the prevailing standards for documenting large-scale patterns of evolution in the fossil record. However, the secular pattern of relative ecological importance between the bryozoan clades Cyclostomata and Cheilostomata is not reflected fully in compilations of generic diversity or within-fauna species richness, and the delayed ecological recovery of the Cheilostomata after the mass extinction at the Cretaceous-Tertiary boundary is missed entirely. These observations demonstrate that evolutionary success and ecological dominance can be decoupled and profoundly different, even over tens of millions of years.

Taxonomic diversity, or richness (1, 2), is the current paradigm used to describe how Earth's biota has changed over time. An alternative approach examines patterns in biological activity or habitat structure (3, 4), but this has rarely been associated with taxonomic diversity. Here, we describe a different approach. We compiled data on skeletal mass of two coexisting marine bryozoan clades (Cyclostomata and Cheilostomata) to measure one aspect of relative local ecological dominance over geological time (5). Dominance is usually measured by the abundance of a group of organisms relative to co-occurring groups, or less often by the relative effect of a group on energy flow within a community (6). Species are not equally abundant or important energetically, so lists of species alone may not reflect dominance. Moreover, despite calls for recognizing the importance of abundance in large-scale evolutionary

patterns (7), there have been few applications (4, 8).

We compared bryozoan abundance data spanning the past 150 million years with two measures of taxonomic diversity to assess the degree of correspondence between the evolutionary success and ecological importance, or dominance, of the two clades on continental shelves, where they have similar ecological distributions (9). During the past 150 million years, cheilostome bryozoans radiated to an extent comparable with the euteleost fishes, neogastropods, and echinoids (2), whereas diversification of cyclostome bryozoans was arrested.

Cyclostome bryozoans survived the severe crises at the end-Permian and Triassic mass extinctions that removed the other stenolaemate bryozoan clades that had much higher Paleozoic diversities (10). Cyclostome genera increased from four in the Early Jurassic [Hettangian; 206 to 202 million years ago (Ma)] to a maximum of 176 in the latest Cretaceous (Maastrichtian; 71 to 65 Ma). Cheilostomes did not appear until the Late Jurassic and increased from four genera in the mid-Cretaceous (Aptian; 121 to 112 Ma) to a maximum of 178 in the Maastrichtian. The Cretaceous-Tertiary (K-T) extinction resulted in a decrease to 111 genera of cheilostomes and to 83 of cyclostomes by the late Paleo-

F. K. McKinney, Department of Geology, Appalachian State University, Boone, NC 28608-2067, USA. S. Lidgard, Department of Geology, Field Museum, Roosevelt Road at Lake Shore Drive, Chicago, IL 60605, USA. J. J. Sepkoski Jr., Department of the Geophysical Sciences, University of Chicago, Chicago, IL 60637, USA. P. D. Taylor, Department of Palaeontology, The Natural History Museum, Cromwell Road, London SW7 5BD, UK.

*To whom correspondence should be addressed. E-mail: mckinneyfk@appstate.edu